Met Office

The Met Office Unified Model GA7.2GL8.1 and GA7.2.1GL8.1.1 configurations: Developments from GA7GL7

Forecasting Research Technical Report No: 654

https://doi.org/10.62998/yrta1217

October 2023

M. R. Willett[1], M. E. Brooks[1], J. M. Edwards[1], A. P. Lock[1], A. J. Malcolm[1], E. H. Müller[2], and W. J. Tennant[1]

[1]Met Office, FitzRoy Road, Exeter, Devon, EX1 3PB, United Kingdom

[2]Department of Mathematical Sciences, University of Bath, BA2 7AY, United Kingdom

Abstract

The Unified Model and JULES are used in defined Global Atmosphere and Global Land configurations to simulate the global atmosphere-land system at the Met Office and at other UM partners. GA7.0GL7.0 was frozen in 2016. However, the NWP performance of this trunk configuration was considered to be unacceptable. The NWP specific branches, GA7.2GL8.1 and GA7.2.1GL8.1.1, were subsequently developed by bringing forward a limited number of changes from the next trunk configuration, GA8GL9. These changes included modifications to the land surface, boundary layer and convection parameterizations and are detailed in this report. The performance of GA7.2GL8.1/GA7.2.1GL8.1.1 was substantially better than GA7GL7 across almost all NWP verification scores and data assimilation metrics. GA7.2GL8.1 was consequently implemented in Parallel Suite 43 (PS43) in December 2019 and followed by GA7.2.1GL8.1.1 in PS44 in December 2020. This remained operational until PS45 in May 2022 when it was replaced by GC4 (GA8GL9 coupled to the GO6 ocean configuration).

1 Introduction

The Unified Model (UM) and JULES are used in defined Global Atmosphere (GA) and Global Land (GL) configurations to simulate the global atmosphere-land system at the Met Office and other UM partners. The GA/GL development process is described in Walters *et al.* (2011). Each subsequent GA/GL configuration is built upon the previous configuration. For example, GA7.0GL7.0 (Walters *et al.* (2019)), is built upon the previous configuration GA6.0GL6.0 (Walters *et al.* (2017)). Each GA/GL configuration is designed for use across all timescales and global resolutions and hence is assessed in terms of both its climate and NWP performance. Branch configurations may be developed from the GC/GA/GL trunks for use in specific applications when the performance of the trunk configuration is deemed to be unacceptable. These will usually include a small number of tunings and science developments pulled forward from the next development cycle.

The NWP performance of GA7.0GL7.0 was considered to be unacceptable relative to the operational configuration at the time, GA6.1GL6.1. Consequently, the NWP specific configuration, GA7.2GL8.1, was developed. Note that GA7.2 is developed from GA7.0 and not from the climate specific branch GA7.1.

GL8.0 was developed from GL7.0 and was defined in 2018. It includes improvements to sea-ice drag and the representation of snow grains. GL8.1 is the aggregate tile version of GL8. GL8.1 became the operational global NWP land surface model in September 2018; initially it was used in combination with GA6.1 and since December 2019 it has been used in combination with GA7.2.

GA7.2GL8.1 became the operational global NWP atmosphere model in December 2019. In December 2020 it was replaced by GA7.2.1GL8.1.1 which included several updates that addressed several specific forecast issues rather than wider forecast performance. This configuration remained operational until May 2022 when it was replaced by GC4 (GA8GL9 coupled to the ocean model).

For brevity in this document the suffix ".0" will be dropped when referring to the trunk configurations (GA7.0, GL7.0, GA8.0, GL8.0, GL9.0).

Section 2 describes the science and technical changes made between GA7GL7 and GA7.2GL8.1/ GA7.2.1GL8.1.1. An evaluation of performance of these branch configurations is given in Section 3.

2 Developments since GA7GL7

The scientific and technical changes added to GA7GL7 to create GA7.2GL8.1/GA7.2.1/GL8.1.1 are detailed below. The configuration in which the change was first included (GA7.2, GA7.2.1, GL8, GL8.1 or GL8.1.1) and the GMED ticket under which the change is documented are given in the section header. All of the changes listed below were subsequently included in GA8GL9 apart from the R_det tuning where a different value was used, and shear-dominated planetary boundary layer (PBL) version where an similar but updated option was used.

2.1 Land surface and hydrology

2.1.1 Revised Roughness Parametrization for Marginal Ice (GL8; GMED ticket #194)

The parametrization of the roughness of marginal ice (i.e. the transition zone between pack ice and open sea) was updated in GL8. The following changes were made:

- Previously the exchange and drag coefficients over sea-ice were interpolated between values representative of pack ice, the marginal ice and open sea. In GL8 this is replaced by explicit

representation of form drag for marginal ice from Lupkes *et al.* (2012), which was validated by Elvidge *et al.* (2016), and using the extension from Lupkes and Gryanik (2015) to account for stability.

- The conductivity of snow on sea-ice is reduced from $0.50\,\mathrm{Wm^{-1}K^{-1}}$ to $0.256\,\mathrm{Wm^{-1}K^{-1}}$ to be consistent with the relationship between snow conductivity and density used in the multilayer snow scheme taken from Calonne *et al.* (2011) and the assumed density for snow on sea ice ($330\,\mathrm{kgm^{-3}}$).
- The conductivity of sea ice is reduced to from $2.63\,\mathrm{Wm^{-1}K^{-1}}$ to $2.09\,\mathrm{Wm^{-1}K^{-1}}$

Renfrew *et al.* (2019) evaluated the changes to the marginal ice drag. They demonstrated that biases and root mean square errors (RMSEs) in temperature and winds were reduced with respect to aircraft observations both over and downstream of the marginal ice zone.

2.1.2 Modifications to the rate of growth of snow grains (GL8; GMED ticket #251)

The size of snow grains affects the albedo of the snow with larger grains being darker. Previous configurations used the parametrization of snow grains from Marshall (1989) which was developed using continental data and did not represent the very low temperatures of Antarctica. In GL8 this is replaced by the equitemperature (ET) part of the scheme described by Taillandier *et al.* (2007) which predicts a slower rate of growth at colder temperatures, so increasing the albedo under typical Antarctic conditions. In addition, the calculation of the grain size during relayering of the snow pack has been modified to make it more consistent with conservation of specific surface area. Increasing the albedo over Antarctica reduces the near surface temperatures; this ultimately results in reduced circulation errors and substantially improved forecast performance in the southern hemisphere in austral summer. Increasing the albedo over Antarctica increases the error slightly relative to CERES-EBAF (this can be seen in fig 8), but it is believed that CERES-EBAF is too dark in this region (J. M. Edwards, personal communication, August 2023).

2.1.3 Drag at High Windspeeds (GL8.1.1; GMED ticket #324)

Although the precise behaviour of the drag at high wind speeds is not fully understood, it is clear that extrapolating standard parametrizations from lower wind speeds gives excessive drag. Indeed, experimental evidence shows that the drag not only saturates at higher wind speeds but actually decreases as the wind speed increases (Donelan *et al.* (2004), Donelan (2018) and Curcic and Haus (2020)). This change limits the drag to 3×10^{-3} when the neutral wind speed is below $33\,\mathrm{ms^{-1}}$, and gradually reduces it between wind speeds of $33\,\mathrm{ms^{-1}}$ and $55\,\mathrm{ms^{-1}}$ where it reaches a limiting value of 2×10^{-3}. This provides good consistency with the experimental estimates. The primary benefit of this development is seen in simulations of tropical cyclones at high resolutions where the drag is reduced and predicted wind speeds are beneficially increased.

2.1.4 Switch to aggregate surface tile (GL8.1; GMED ticket #480)

As was the case for earlier NWP branches (GL3.1 and GL6.1) it has been necessary to use an aggregate surface tile (see for example Walters *et al.* (2019)) rather than the 9-tiles used in GL7. With the aggregate tile the properties of each tile type are aggregated into a single tile from which surface fluxes are calculated. A description of the aggregate tile is given in Walters *et al.* (2019).

2.2 Boundary layer

2.2.1 Increase the non-linear solver term (puns) for unstable boundary layers (GA7.2; GMED ticket #290)

The puns parameter controls the boundary layer (BL) implicit solver in unstable boundary layers, specifying an assumed level of non-linearity in the calculation of the diffusion coefficient in the column when the surface buoyancy flux is positive (see Wood *et al.* (2007)). Higher values of puns give greater stability but can give excessive damping. As a result, a weak non-linearity value for puns of 0.5 has been used in GA7GL7, consistent with the non-local nature of the diffusion coefficient calculation in unstable BLs. However, occasional failures have been seen with this setting when there is a column of extremely high winds extending well above the depth of the diagnosed unstable BL depth. The instability is likely generated above the BL where a significantly more non-linear (Richardson-number dependent) diffusion coefficient calculation is used. This hypothesis is supported by the fact that increasing puns to 1.0 greatly reduces the likelihood of this failure mechanism. Additional testing has shown negligible impact on forecast performance, including for example, in the diurnal evolution of the convective BL.

2.2.2 Shear-dominated PBL version 2 (GA7.2; GMED ticket #479)

The shear dominated BL type allows shear generated turbulence to overrule the thermodynamic parcel ascent diagnosis of the mixed layer depth, which in turn allows turbulent mixing to extend into regions of weak static stability and to potentially inhibit the formation of cumulus. This change modifies the ”dynamic diagnosis” of shear driven layers as applied to sea points. In particular, it now requires that the bulk surface stability is near neutral. If these conditions are met then the surface based mixed layer depth is reset to zero and cumulus diagnosis is set to false. This change results in shear dominated BLs being diagnosed less frequently, which on average reduces the BL depth, with compensating increases in well-mixed and cumulus BL types. This change slightly improves the forecast performance due to small but systematic improvements in the lower tropospheric temperature structure.

2.3 Convection

2.3.1 Revised forced detrainment calculation (GA7.2; GMED ticket #207)

Forced adaptive detrainment is a mechanism within the convection scheme that represents an ensemble of plumes with a range of buoyancies whilst only explicitly calculating the mean buoyancy (Derbyshire *et al.*, 2011). It preferentially detrains the part of the distribution that is no longer buoyant and thereby increases the buoyancy of the remaining parcel albeit at the expense of reduced mass flux. In previous configurations, when the air within the convective updraught became unsaturated and forced detrainment was triggered, the humidity of the parcel undergoing forced detrainment was assumed to have the parcel mean humidity. The forced detrainment was, consequently, unable to modify the humidity of the remaining parcel and it would remain unsaturated. This usually results in the updraught terminating as soon as it becomes unsaturated even though convection may still have been viable for some fraction of the distribution.

This change improves the treatment of subsaturated forced detrainment by assuming the detrained parcel has a humidity equal to that of the mean of the environment and parcel humidities. This allows subsaturated force detrainment to increase the humidity of the remaining parcel and hence increases the likelihood of convection continuing. It should be noted that the scheme does not support purely dry convection: latent heat release is required during some part of ascent otherwise it will be ignored.

The effect of this change is to allow convection to become slightly deeper. This ultimately results in a warming of $\sim 0.1\,\mathrm{K}$ at around 600 and 100 hPa, and a $\sim 0.1\,\mathrm{K}$ cooling at around 250 hPa.

2.3.2 Switch off the convective water and energy correction for GA8 (GA7.2; GMED ticket #474)

The 6a convection scheme, which was added in GA7, includes a correction to the water and energy that was not included in the previous version of convection scheme. Even without the correction, the water and energy conservation in the 6a scheme is very good, but small errors can be generated because it assumes hydrostatic balance and a shallow atmosphere (it uses pressure levels) whilst the model dynamics is non-hydrostatic and assumes a deep atmosphere. This correction step, however, tends to produce a small ($\sim 0.1\,\mathrm{K}$) tropospheric warming that results in a negative impact on verification scores. For that reason, the correction is pragmatically switched off in GA7.2. The overall conservation of energy and water in the model is no worse with this correction switched off. This is probably because it introduces a small compensating error that offsets other sources of non-conservation within the model.

2.3.3 Limit CAPE timescale to reduce convectively coupled waves (GA7.2.1; GMED ticket #476)

GA7 introduced a CAPE timescale that is dependent on the large-scale vertical velocity. Larger vertical velocities result in shorter CAPE timescales with the lower limit being the convection timestep which is half the model timestep; at N1280 the minimum CAPE timescale would be 2 minutes. However, it was subsequently noted that at higher resolutions this closure increases the frequency of spurious fast-moving, convectively coupled waves. This issue is greatly mitigated in GA7.2.1 by simply limiting the minimum CAPE timescale to 30 minutes.

2.4 Dynamical formulation and discretisation

2.4.1 Multigrid solver (GA7.2.1; GMED ticket #531)

The UM uses a nested iterative structure for each timestep which is split into inner and outer loops (Wood *et al.* (2014)). At the end of the inner-loop it is necessary to solve the Helmholtz problem for the pressure increment. In GA7.2.1 a new multigrid solver is used in the Helmholtz solver.

Multigrid (for an introduction see e.g. Wesseling (1995)) is an iterative numerical technique for the efficient solution of the system of sparse linear equations that arises in semi-Lagrangian timestepping. By using a series of coarser and coarser numerical grids, the solution to the discretised equations can be found while performing much less computational work and by passing much less information between processors (see Buckeridge and Scheichl (2010) for the adaptation of multigrid to latitude-longitude grids and Müller and Scheichl (2014) for a general review of multigrid in NWP). These attributes mean that for most cases multigrid is faster than the postconditioned variant of van der Vorst's bi-conjugate gradient stabilized (BiCGstab) method (van der Vorst (1992)) used in GA7. Since the solver is independent of the system of equations that is to be solved and all iterative schemes reduce the numerical error below a pre-defined tolerance, this change does not represent a fundamental difference in physical representation: both the multigrid solver and the existing method produce a solution of the sparse linear system within the specified accuracy. The multigrid scheme has very small impact on overall forecast performance but does produce noticeably smoother solutions at the poles.

2.5 Corrections

2.5.1 Correction to exchange coefficient in dust deposition (GA7.2; GMED ticket #173)

This change fixes a bug in the calculation of the surface layer friction velocity, U^*, where it appears in the calculation of surface layer resistance for surface deposition of dust. The impact is to generate a larger exchange coefficient for surface deposition leading to a small reduction in low level dust concentration.

2.5.2 Correction to zh diagnostic with forced cumulus (GA7.2; GMED ticket #301)

The forced cumulus option, first used in GA7, erroneously sets the prognostic boundary layer depth variable, zh, to just the non-local layer depth rather than the maximum of local and non-local depths. This results in the boundary layer depth diagnostic erroneously being overwritten with this non-local depth (which is zero at night, for example). It also leads to errors in the actual model evolution because zh is used elsewhere in the implicit BL and on the next timestep in the convection diagnosis. This change corrects this error and consequently replaces the non-local PBL depth with the physical PBL depth in the calculation of BL frictional heating, the BL velocity scale, surface layer depth and maximum buoyancy perturbation in the convection diagnosis as well as in the boundary layer depth diagnostics. In practice, only the change to frictional heating has a non-negligible effect on model evolution.

2.5.3 Fix water conservation in PC2 ice/water partition in convection (GA7.2; GMED ticket #434)

PC2 retrospectively re-partitions the original forced detrainment increments for liquid and frozen water within the convection scheme. In GA7 this process assumes that convective parcel cannot have mixed phase: this is only true, however, above the initiation level because at cloud base the convective parcel is initialised with environmental liquid and frozen water and both phases can co-exist. Therefore, if the initial level has mixed phase and there is forced detrainment between the initial level and the level above, the scheme will not exactly conserve water (although the error is typically very small). This change corrects the logic within the scheme to allow for mixed phased condensate within PC2's re-partition of the forced detrainment increments of liquid and frozen water. Although this change substantially improves the conservation of water it has a negligible effect on the model's forecast performance.

2.5.4 Set temporary logicals to .true. (GA7.2.1GL8.1.1; GMED ticket #484)

In the UM "temporary logicals" are used to protect fixes to the UM that significantly alter science configurations. The protection is provided so that a defined GA/GL/GC configuration is scientifically consistent across a limited number of UM releases. From a technical perspective it is desirable to set as many temporary logicals to true at each GA/GL configuration because this will aid the retirement of the logicals and simplify the code. From a scientific perspective it is desirable to set them to true because that will fix bugs in the code and enhance the scientific integrity of the model. For GA7.2.1GL8.1.1 all available temporary logicals available at the time of the freeze of GA8GL9 (which is those that existed in UM at vn11.4) were set to true. Not all of these fixes are relevant to NWP applications. A list of relevant fixes plus a brief description is given in Table 1. These corrections have a negligible effect on the model's evolution.

Scheme	Variable	Parameter Description
JULES	l_fix_albsnow_ts	The two-stream scheme to calculate the albedo of snow in JULES contains a bug in the calculation of the reflection coefficient that renders very thin layers of snow too reflective. This is fixed when set to True.
	l_fix_alb_ice_thick	When set to true fixes a bug in ice thickness used for sea ice albedo calculation.
	l_fix_osa_chloro	Correct the units of chlorophyll in the ocean surface albedo.
Reconfiguration	l_fix_rcf_mlsnow_icefreemax	Reconfiguration may cause ice points on the input grid to be converted into ice-free points on the output grid, but such points are likely to acquire large snow mass and it is usually desirable to limit these. This fix applies the correct limit.
	l_roughnesslength_fix	Fixes possible unrealistic 10m winds near coasts on the first timestep due to land z0 values being interpolated over the sea in the reconfiguration.
IAU	l_fix_iau_rim_density	Fix a bug affecting rim density values when running the IAU.
Convection	l_fix_ccb_cct	Uses a simpler and more robust calculation of convective cloud base and top.
Stochastic	l_fix_rp_shock_amp	Fix to shock amplitude in the AR1 process of the random parameters scheme.
	l_fix_lsp_incs_to_spt	When set to true this option allows the stochastic parametrized tendencies (SPT) scheme to see the affects of the mixed-phase turbulent microphysics.

Table 1: Temporary logicals that are applicable to NWP applications and set to true as part of #484

2.6 Tuning

2.6.1 Reduce R_Det for GA7.2 (GA7.2; GMED ticket #478)

R_Det controls the level of "adaptivity" in the convection scheme's adaptive forced detrainment (Derbyshire *et al.* (2011)). As such it controls the assumed shape and width of the convective parcel buoyancy probability density function (PDF) with smaller values indicating a narrower PDF. In GA7.2 R_Det is reduced from 0.8 to 0.7. This is a tuning but it does bring the value closer to that estimated in Derbyshire *et al.* (2011). Decreasing R_Det cools the upper tropical troposphere by $\sim 0.2\,\mathrm{K}$ whilst slightly warming the mid tropical troposphere by $\sim 0.1\,\mathrm{K}$.

3 Evaluation

3.1 NWP

Three-month Data Assimilation (DA) deterministic only trials at N640 were run for GA7.2.1GL8.1.1 and GA7GL7 for September, October and November (SON) 2019. The equivalent GA7.2GL8.1 trial has not been run, but other testing demonstrated that there is little difference in performance between the two branch configurations. The verification with respect of own analysis and observations is summarised in Figure 1. It can be readily seen that GA7.2.1GL8.1.1 has lower root mean square errors (RMSEs) than GA7GL7 when measured against their own analyses for almost all parameters and at all forecast times. When measured against observations this signal is not quite as strong but still indicates that GA7.2.1GL8.1.1 is substantially outperforming GA7GL7. Within the data assimilation, the GA7.2.1GL8.1.1 background forecast is in better agreement with the large majority of observation types

(Figure 2) than the GA7GL7 background forecast.

The RMSEs in temperature are reduced for most levels in both the mid-latitudes and the tropics when verified against own analysis (e.g. Figures 3 and 4) and sondes (not shown). The exception is in the tropics at around 250 hPa where the cooling, which is primarily the result of the changes to the convection scheme, peaks and results in a cold bias of up to $\sim 0.3\,\mathrm{K}$. In GA7.2.1GL8.1.1 this cold bias has saturated by T+72: in GA7GL7, however, a warm bias develops in the later half of the forecast which is comparable in magnitude to GA7.2.1GL8.1.1's cold bias. Below $\sim$ 400 hPa the temperature biases are either reduced or are no worse than in GA7GL7.

The root mean square vector errors (RMSVEs) in the horizontal winds are reduced at most levels and in both the mid-latitudes and the tropics when verified against own analysis (e.g. Figures 5 and 6) and sondes (not shown). The wind speed biases are generally improved. There is a large reduction in a fast bias at 100-150 hPa, which is attributable to convection changes cooling the upper troposphere, that leads to a large reduction in RMSVE at these levels.

By almost all measures GA7.2.1GL8.1.1 is a substantial improvement on GA7GL7 in an NWP context with the only detriment being the development of a small cold bias in the upper tropical troposphere.

3.2 Climate

Although GA7.2GL8.1 is an NWP branch, it is still desirable to assess its climate performance. This helps to ensure that any improvements that we see in NWP do not come at the expense of a degraded climate and hence would be difficult to reintegrate into the GA trunk. Furthermore, if the climate were to be degraded then this would suggest that the NWP improvements are not necessarily for the right reasons and we obviously wish the check this. To that end, N96 AMIP tests of GA7.2GL8 and GA7GL7 were compared. The annual mean precipitation, outgoing shortwave radiation (OSW) and outgoing longwave radiation (OLR) from GA7.2GL8 are compared to GA7GL7 in figures 7, 8 and 9 respectively. There all small and systematic changes in all the fields but overall the biases are reduced against the observational estimates. The overall impact of GA7.2GL8 on the climate is relatively small but generally positive.

4 Summary

The performance of GA7GL7 was considered to be unacceptable for operational NWP implementation. GA7.2.1GL8.1.1/GA7.2.1GL8.1.1 are the NWP branches of GA7GL7. They brought forward a limited number of changes that were subsequently included in next trunk configuration the global atmosphere and global land model, GA8GL9. The performance of GA7.2.1GL8.1.1/GA7.2.1GL8.1.1 was substantially better than GA7GL7 across almost all NWP verification scores and Data Assimilation metrics. GA7.2GL8.1 was consequently implemented in Parallel Suite 43 (PS43) in December 2019 followed by GA7.2.1GL8.1.1 in PS44 in December 2020. This remained operational until PS45 in May 2022 when it replaced by GC4 (GA8GL9 coupled to the GO6 ocean configuration).

5 References

References

Buckeridge, S. and Scheichl, R. 2010. Parallel geometric multigrid for global weather prediction. *Numerical Linear Algebra with Applications* **17**: 325–342.

Calonne, N., Flin, F., Morin, S., Lesaffre, B., Rolland du Roscoat, S., and Geindreau, C. 2011. Numerical and experimental investigations of the effective thermal conductivity of snow. *Geophys. Res. Lett.* **38**: L23501.

Curcic, M. and Haus, B. K. 2020. Revised estimate of ocean surface drag in strong winds. *Geophys. Res. Lett.* **47**.

Derbyshire, S. H., Maidens, A. V., Milton, S. F., Stratton, R. A., and Willett, M. R. 2011. Adaptive detrainment in a convection parametization. *Q. J. R. Meteorol. Soc.* **137**(660): 1856–1871.

Donelan, M. A. 2018. On the decrease of the oceanic drag coefficient in high winds. *Journal of Geophysics Research: Oceans* **123**.

Donelan, M. A., Haus, B. K., Reul, N., Plant, W. J., Stiassne, M., Graber, H. C., Brown, O. B., and Saltman, E. S. 2004. On the limiting aerodynamic roughness of the ocean in very strong winds. *Geophys. Res. Lett.* **31**.

Elvidge, A. D., Renfrew, I. A., Weiss, A. I., Brooks, I. M., Lachlan-Cope, T. A., and King, J. C. 2016. Observations of surface momentum exchange over the marginal ice zone and recommendations for its parametrisation. *Atmos. Chem. Phys.* **16**: 1545–1563.

Lupkes, C. and Gryanik, V. M. 2015. A stability-dependent parametrization of transfer coefficients for momentum and heat over polar sea ice to be used in climate models. *J. Geophys. Res. Atmos.* **120**: 552–581.

Lupkes, C., Gryanik, V. M., Hartmann, J., and Andreas, E. L. 2012. A parametrization, based on sea ice morphology, of the neutralatmospheric drag coefficients for weather predictionand climate models. *J. Geophys. Res. Atmos.* **117**.

Marshall, S. E. 1989. A physical parameterization of snow albedo for use in climate models. Ph.D. thesis University of Colorado Boulder. NCAR Cooperative thesis 123.

Müller, E. H. and Scheichl, R. 2014. Massively parallel solvers for elliptic partial differential equations in numerical weather and climate prediction. *Q. J. R. Meteorol. Soc.* **140**: 2608–2624.

Renfrew, I. A., Elvidge, A. D., and Edwards, J. M. 2019. Atmospheric sensitivity to marginal-ice-zone drag: global and local responses. *Q. J. R. Meteorol. Soc.* **145**: 1165–1179.

Taillandier, A.-S., Domine, F., Simpson, W. R., Sturm, M., and Douglas, T. A. 2007. Rate of decrease of the specific surface area of dry snow: Isothermal and temperature gradient conditions. *J. Geophys. Res. Earth Surf.* **112**: F03003.

van der Vorst, H. A. 1992. Bi-CGSTAB: A Fast and Smoothly Converging Variant of Bi-CG for the Solution of Nonsymmetric Linear Systems. *SIAM J. Sci. Stat. Comput.* **13**: 631–644.

Walters, D., Baran, A., Boutle, I., Brooks, M., Earnshaw, P., Edwards, J., Furtado, K., Hill, P., Lock, A., Manners, J., Morcrette, C. Mulcahy, J., Sanchez, C., Smith, C., Stratton, R., Tennant, W., Tomassini, L., Van Weverberg, K., Vosper, S., Willett, M., Browse, J., Bushell, A., Dalvi, M., Essery, R., Gedney, N., Hardiman, S., Johnson, B., Johnson, C., Jones, A., Mann, G., Milton, S., Rumbold, H., Sellar, A., Ujiie, M., Whitall, M., Williams, K., and Zerroukat, M. 2019. The Met Office Unified Model Global Atmosphere 7.0/7.1 and JULES Global Land 7.0 configurations. *Geosci. Model Dev.* **12**: 1909–1963.

Walters, D. N., Best, M. J., Bushell, A. C., Copsey, D., Edwards, J. M., Falloon, P. D., Harris, C. M., Lock, A. P., Manners, J. C., Morcrette, C. J., Roberts, M. J., Stratton, R. A., Webster, S., Wilkinson, J. M., Willett, M. R., Boutle, I. A., Earnshaw, P. D., Hill, P. G., MacLachland, C., Martin, G. M., Moufouma-Okia, W., Palmer, M. D., Petch, J. C., Rooney, G. G., Scaife, A. A., and Williams, K. D. 2011. The Met Office Unified Model Global Atmosphere 3.0/3.1 and JULES Global Land 3.0/3.1 configurations. *Geosci. Model Dev.* **4**: 919–941.

Walters, D. N., Brooks, M., Boutle, I., Melvin, T., Stratton, R., Vosper, S., Wells, H., Williams, K., Wood, N., Allen, T., Bushell, A., Copsey, D., Earnshaw, P., Edwards, J., Gross, M., Hardiman, S., Harris, C., Heming, J., Klingman, N., Levine, R., Manners, J., Martin, G., Milton, S., Mittermaier, M., Morcrette, C., Riddick, T., Roberts, M., Sanchez, C., Selwood, P., Stirling, A., Smith, C., Suri, D., Tennant, W., Vidale, P. L., Wilkinson, J., Willett, M., Woolnough, S., and Xavier, P. 2017. The Met Office Unified Model Global Atmosphere 6.0/6.1 and JULES Global Land 6.0/6.1 configurations. *Geosci. Model Dev.* **10**: 1487–1520.

Wesseling, P. 1995. Introduction to multigrid methods. Contractor Report 195045 NASA.

Wood, N., Diamantakis, M., and Staniforth, A. 2007. A monotonically-damping second-order-accurate unconditionally-stable numerical scheme for diffusion. *Q. J. R. Meteorol. Soc.* **133**: 1559–1573.

Wood, N., Staniforth, A., White, A., Allen, T., Diamantakis, M., Gross, M., Melvin, T., Smith, C., Vosper, S., Zerroukat, M., and Thuburn, J. 2014. An inherently mass-conserving semi-implicit semi-Lagrangian discretization of the deep-atmosphere global non-hydrostatic equations. *Q. J. R. Meteorol. Soc.* **140**: 1505–1520.

6 Figures

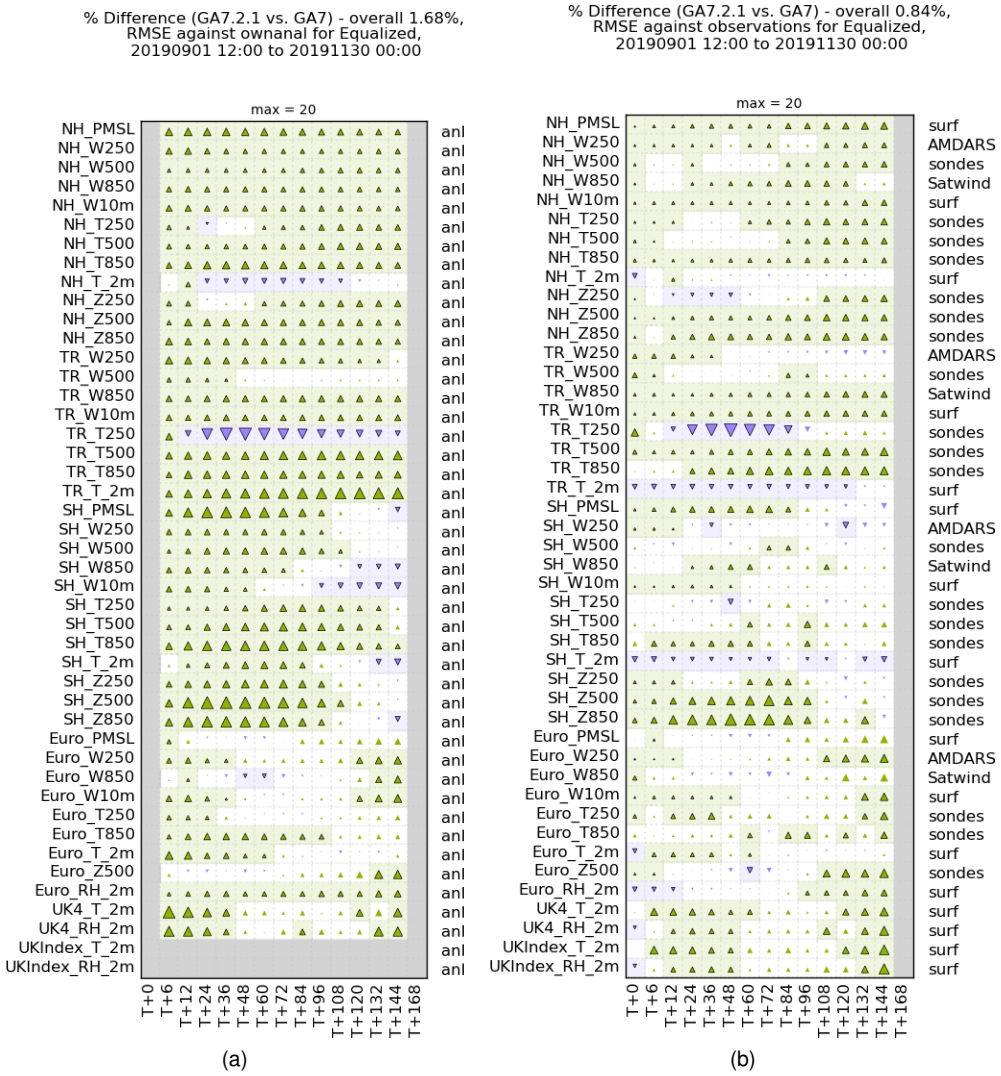

Figure 1: Global evaluation suite scorecards for GA7.2.1GL8.1.1 vs GA7GL7 with respect to (a) own analysis and (b) observations for the three month N640 DA non-hybrid trial for SON 2019. Shaded boxes are statistically significant. Green upward pointing triangles indicate the RMSEs in GA7.2.1GL8.1.1 are reduced relative to GA7GL7, and downward pointing purple triangles indicate where the RMSEs are increased.

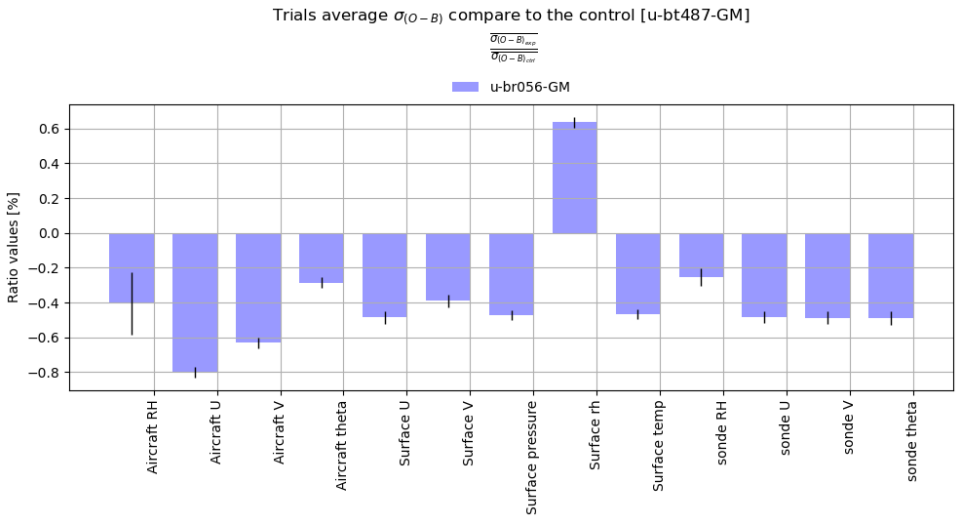

(a)

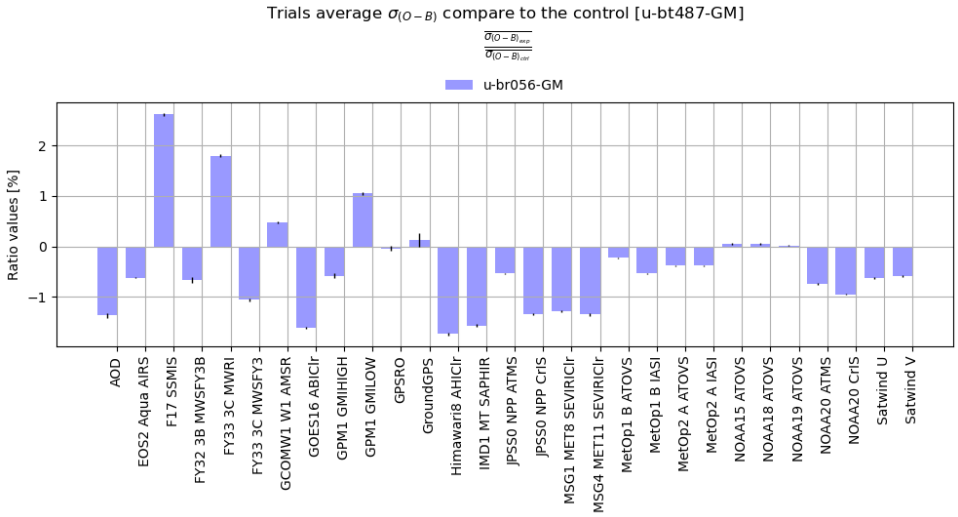

(b)

Figure 2: Data assimilation summary as measured by the percentage change between GA7.2.1GL8.1.1 and GA7GL7 in the standard deviation of observations minus background for (a) conventional observations and (b) satellite observations for the three month N640 DA non-hybrid trial for SON 2019. Negative values indicate that GA7.2.1GL8.1.1 is improved relative to GA7GL7.

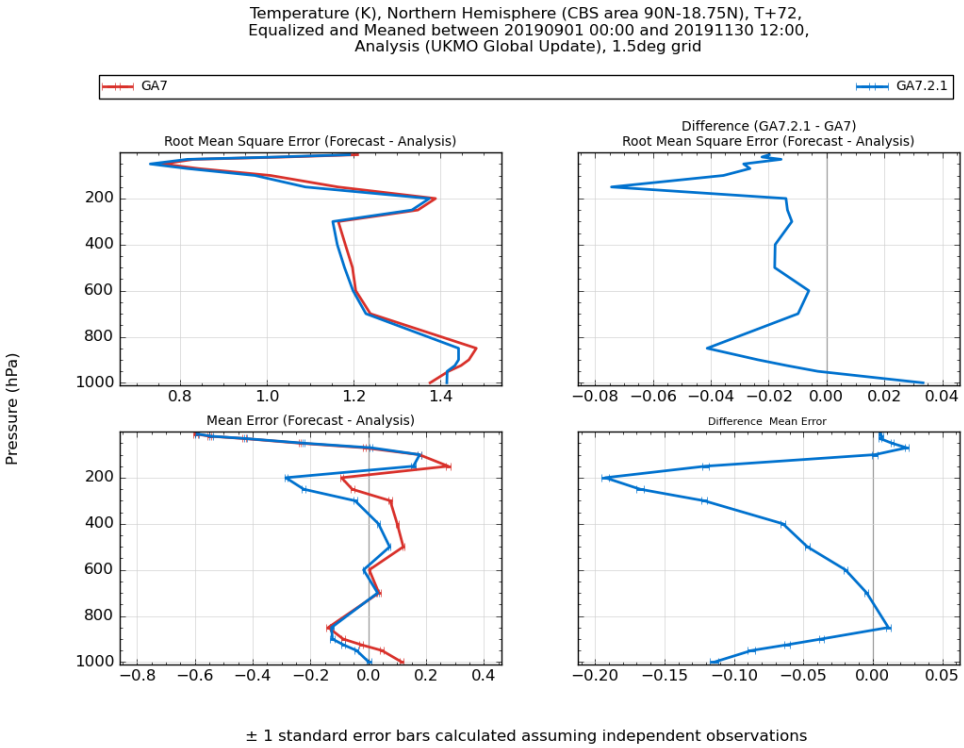

Figure 3: Verification with respect to own analysis of northern hemisphere T+72 temperatures forecasts from GA7.2.1GL8.1 and GA7GL7 showing RMSE (top left), difference in RMSE (top right), bias (bottom left), and difference in mean error (bottom right) for the three month N640 DA non-hybrid trial for SON 2019.

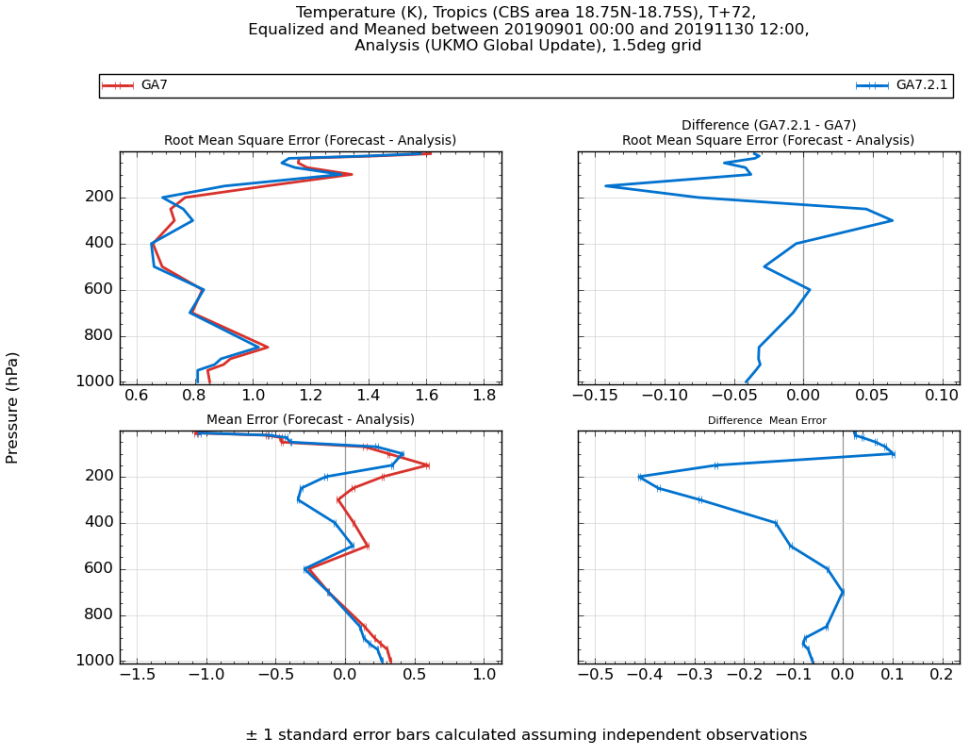

Figure 4: As Figure 3 but for the tropics.

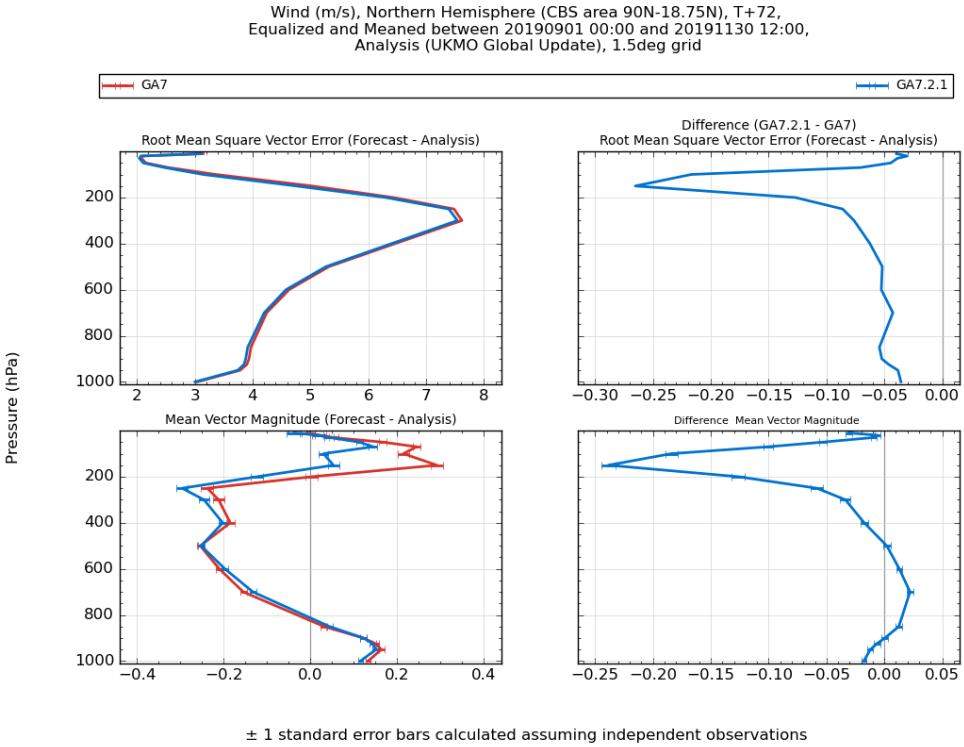

Figure 5: Verification with respect to own analysis of northern hemisphere T+72 wind forecasts from GA7.2.1GL8.1 and GA7GL7 showing RMSE (top left), difference in RMSE (top right), bias (bottom left), and difference in mean error (bottom right) for the three month N640 DA non-hybrid trial for SON 2019.

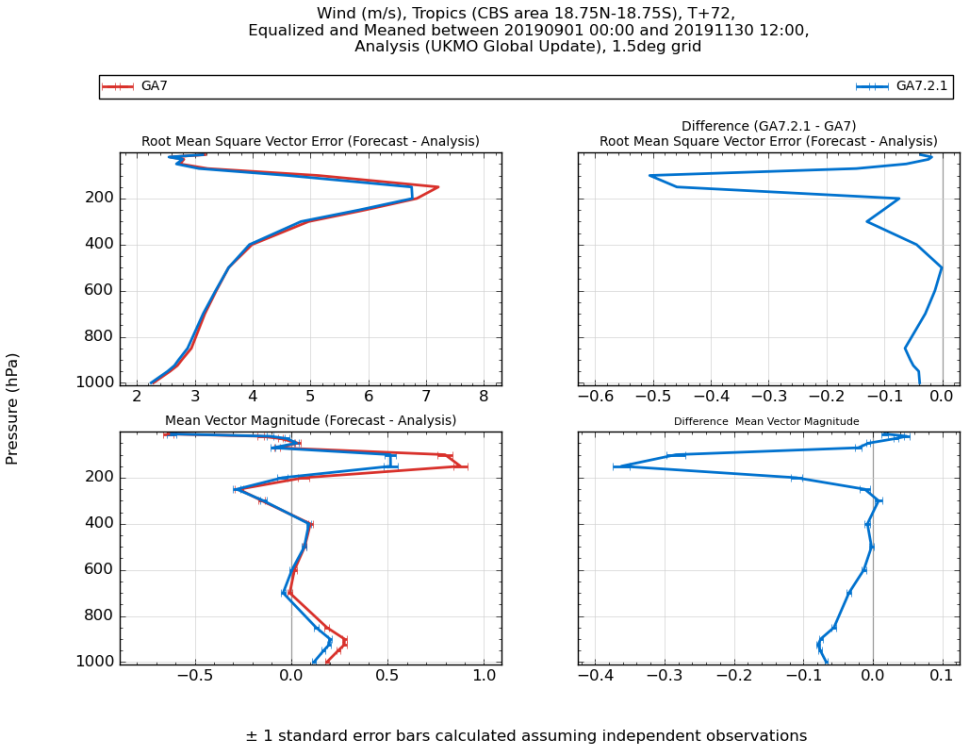

Figure 6: As Figure 5 but for the tropics.

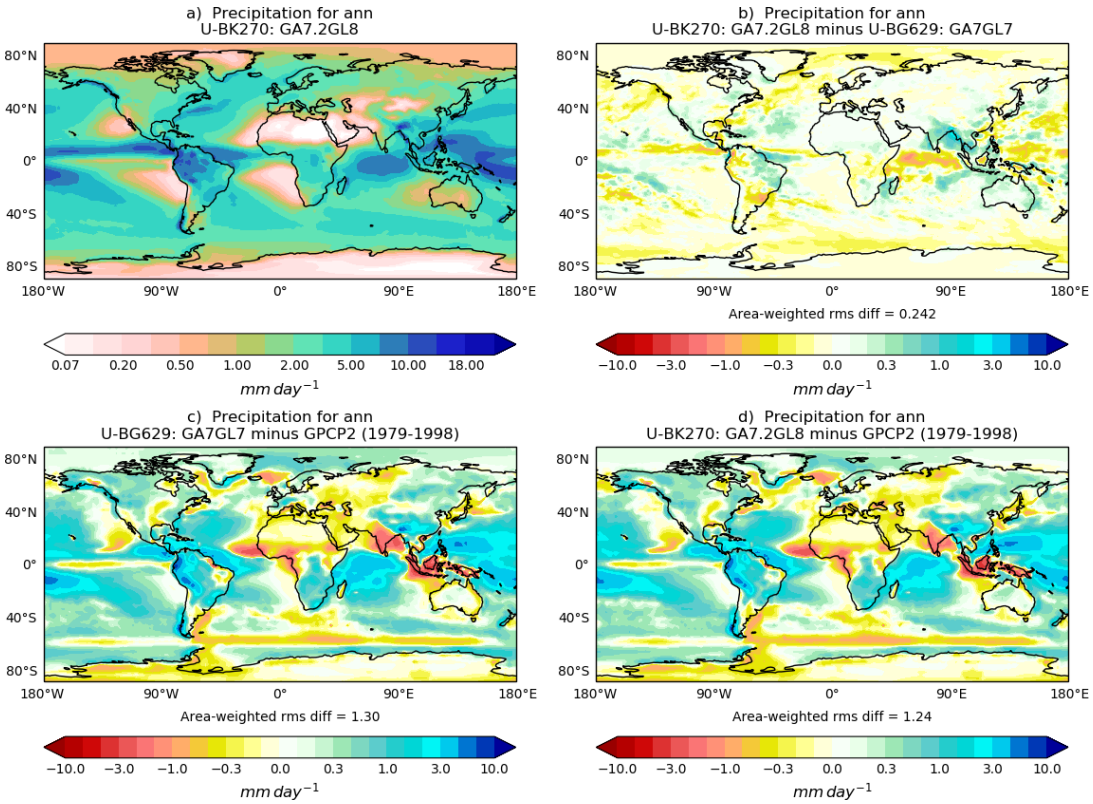

Figure 7: Annual mean precipitation from 20-year N96 simulations using GA7GL7 and GA7.2GL8. The panel shows (top left) mean precipitation from GA7.2GL8, (top right) difference between GA7.2GL8 and GA7GL7, (bottom left) error in GA7GL7 relative to GPCP and (bottom right) error in GA7.2GL8 relative to GPCP.

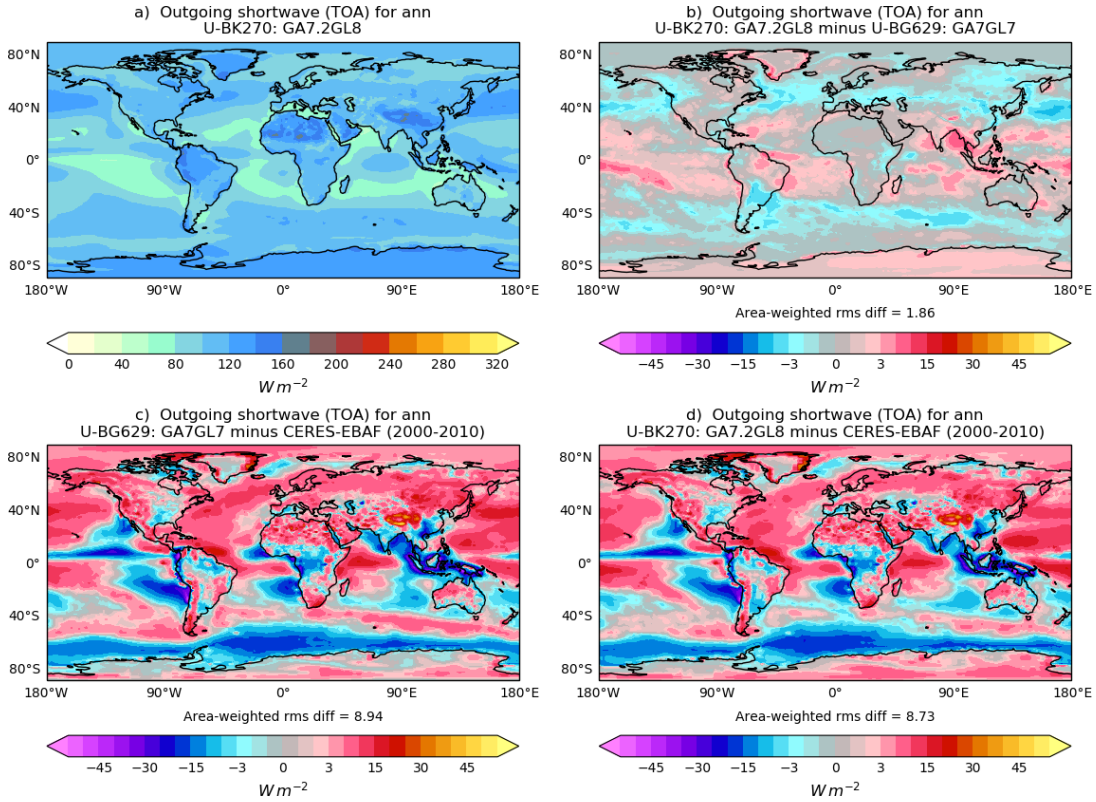

Figure 8: Annual mean outgoing showrtwave radiation from 20-year N96 simulations using GA7GL7 and GA7.2GL8. The panel shows (top left) mean precipitation from GA7.2GL8, (top right) difference between GA7.2GL8 and GA7GL7, (bottom left) error in GA7GL7 relative to CERES-EBAF and (bottom right) error in GA7.2GL8 relative to CERES-EBAF vn2.6.

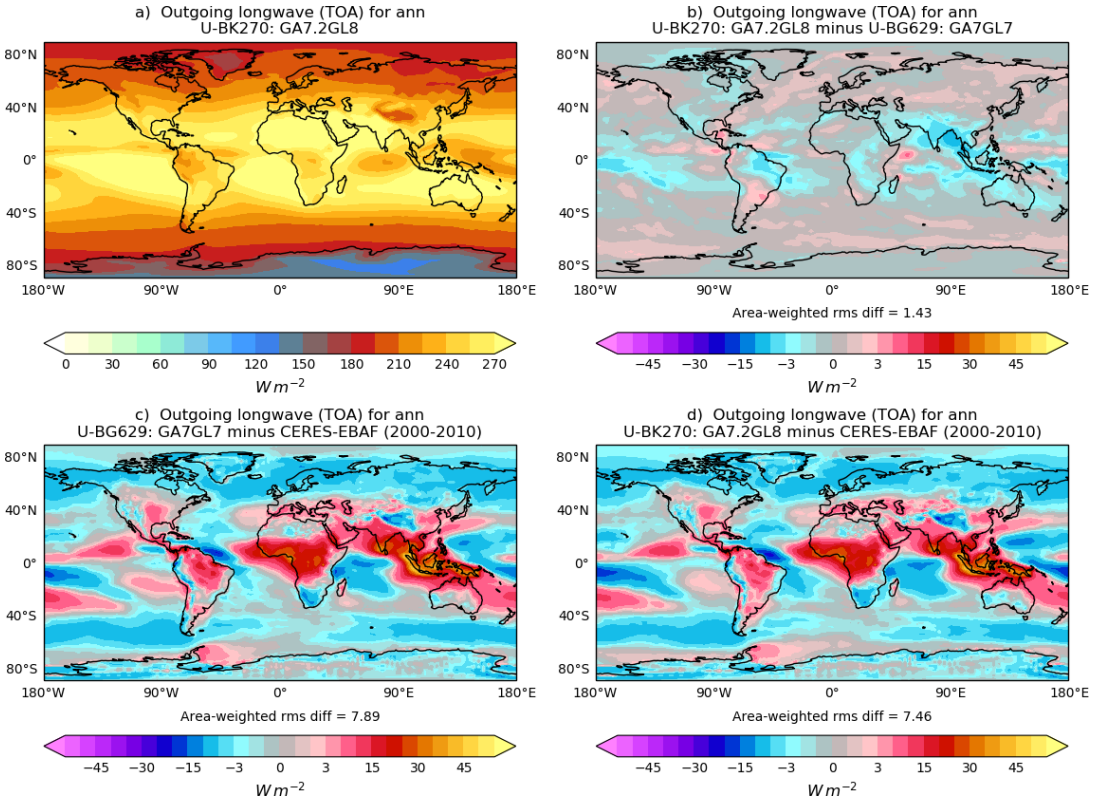

Figure 9: Annual mean outgoing longwave radiation from 20-year N96 simulations using GA7GL7 and GA7.2GL8. The panel shows (top left) mean precipitation from GA7.2GL8, (top right) difference between GA7.2GL8 and GA7GL7, (bottom left) error in GA7GL7 relative to CERES-EBAF and (bottom right) error in GA7.2GL8 relative to CERES-EBAF vn2.6.

Met Office
FitzRoy Road
Exeter
Devon
EX1 3PB
United Kingdom

Produced with the Met Office LaTeX template v3.0.0